Time-resolved experimental and computational study of two-photon laser-induced fluorescence in a hydrogen plasma

H. W. P. van der Heijden, M. G. H. Boogaarts, S. Mazouffre, J. A. M. van der Mullen,* and D. C. Schram
Department of Applied Physics, Eindhoven University of Technology, P.O. Box 513, 5600 MB Eindhoven, The Netherlands
(Received 2 November 1999)

The time profile of the fluorescence light emission of atomic hydrogen in an expanding plasma beam after pulsed excitation with a nanosecond laser is studied, both experimentally and computationally. Ground state H atoms in an expanding Ar-H cascaded arc plasma are excited to the $p=3$ level using two-photon laser excitation at 205 nm. The resulting fluorescence is resolved in time with a fast photomultiplier tube to investigate the occurrence of quenching. A fluorescence decay time of (10 ± 0.5) ns is measured under all circumstances, indicating that there is a complete l mixing of the $p=3$ sublevels. A time-resolved collisional radiative model is developed to model pulsed laser induced fluorescence for a large range of plasma parameters. The model calculations agree well with the experimental results over the entire range of conditions and indicate that two-photon LIF can strongly influence the local electron and ion densities, resulting in a ''self-quenching'' of the laser-induced H fluorescence.

PACS number(s): 52.40.Nk, 52.70.−m, 52.65.−y, 32.50.+d

I. INTRODUCTION

Fluorescence from laser induced two-photon excitation provides a powerful method to measure ground state densities of atoms or molecules with a large energy gap between ground and first excited state. The technique has found important applications in, among other things, combustion and low-temperature plasma research, and has been applied to a variety of species [1–4].

By measuring the fluorescence light emitted from the excited state, a signal proportional to the ground state density is obtained. If the decay of the excited level is purely governed by radiative processes, the proportionality constant is independent of plasma parameters and therefore needs to be calibrated only once. The most common exception to this condition is formed by (electron) collision induced transitions (quenching). These result in a shorter lifetime of the excited state and therefore a lower fluorescence signal. In order to use two-photon laser induced fluorescence (LIF) as a means to study ground state densities, it is necessary to not only calibrate the fluorescence signal, but also to ascertain the absence of quenching. In this work the term quenching is used for the overall collision-induced (thus radiationless) decay of the excited-state population, including both downward and upward transitions (electron excitation).

In our group, two-photon LIF is used to investigate the density of H ground state atoms in an expanding cascaded arc argon-hydrogen plasma, by two-photon excitation of the hydrogen ground state to the $p=3$ state at 205 nm [1]. The excitation is monitored by detection of the resulting fluorescence on the Balmer-α transition at 656 nm. An overview of this scheme is given in Fig. 1.

This article will discuss an experimental and computational investigation of the occurrence of quenching of the H $p=3$ state in the expanding plasma. In order to verify the absence of quenching, the fluorescence radiation from the $3\rightarrow2$ transition is measured as a function of time. By measuring the LIF decay time in the expanding plasma at different distances from the plasma source, a range of hydrogen densities ($10^{17}-10^{20}$ m^{-3}) with electron densities between $10^{16}-2\times10^{18}$ m^{-3} has been investigated.

To be able to confirm the experimental results, a time-dependent collisional radiative model (CRM) [5] has been developed. The model describes the effects of laser induced excitation of the ground state and ionization of the excited states. Results from calculations for the experimental conditions will be compared with experiments. In addition, the model allows us to study the excitation kinetics of the hydrogen system in general, and the effects of two-photon excitation in particular, for a much wider range of plasma conditions. In an ideal LIF experiment, the amount of detected fluorescence will be proportional to the ground state density

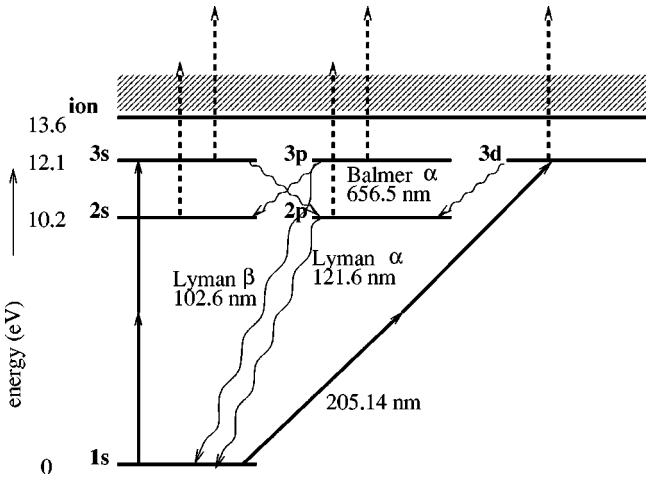

FIG. 1. Scheme of the hydrogen two-photon excitation (solid arrows) from $1s$ to $3s$ and $3d$. The laser photons are also capable of ionizing excited H states (dashed arrows). The Balmer-α 656 nm fluorescence radiation is measured.

*Author to whom correspondence should be addressed. Electronic address: J.J.A.M.v.d.Mullen@phys.tue.nl

n_1. One of the aims of the model is to calculate under which plasma conditions this holds.

The experimental method and setup are described in detail in a separate paper [6], therefore Sec. II gives only a short summary of the setup. Since we measure short signals — decay times of perhaps 10 ns or less if there is quenching — special attention is given to the time-resolved diagnostics. In Sec. III the experimental results are presented and discussed. In Sec. IV the development of the time-resolved CRM is explained while Sec. V presents and discusses the results from model calculations. Finally, some conclusions are given in Sec. VI.

II. EXPERIMENT

The cascaded arc plasma source has been extensively discussed in the literature [7–9]. In this work, the arc was operated at 40 A with 3 slm argon and 0.46 slm H_2 flows. The plasma expands from a nozzle into a roots-blower pumped vacuum vessel with a background pressure of 14 Pa. In the cascaded arc, the plasma is expected to burn on hydrogen whereas argon is mainly present as a buffer gas. Due to the high power density in the cascaded arc, it is expected that a considerable part of H_2 will be dissociated. The determination of the dissociation degree is one of the main goals of the plasma beam H ground state density measurements that are performed in our group [6,10]. The setup is constructed so that the measurements can be made at varying positions in the plasma beam. The electron density n_e will drop substantially as the plasma moves away from the nozzle while the electron temperature T_e is expected to remain close to 0.3 eV.

A frequency doubled Nd:YAG laser (Spectra-Physics GCR230) is used to pump a tunable dye laser (Spectra-Physics PDL-3) producing 615 nm light at 50 Hz. Part of the dye laser light is frequency doubled in a KDP crystal and then mixed with the remaining 615 nm light in a BBO crystal to obtain a 205 nm linearly polarized laser beam. The average laser pulse energy is measured using a calibrated power meter at the beginning of the beam. Behind the plasma an uncalibrated UV sensitive SiC diode is placed in the beam to measure pulse energies on a shot by shot basis. The laser typically produces 0.5 mJ, 5 ns pulses of tunable 205 nm radiation with a spectral bandwidth of 0.2 cm^{-1}. The laser beam is focused into the plasma in a direction perpendicular to the expansion. Two lenses are positioned so that light from the region where the laser beam is focused is imaged with a one-to-one ratio on a slit mask (width 0.4 mm) in a direction again perpendicular to both the laser beam and the expansion axis. The light then passes through a Balmer-α filter and enters the photomultiplier tube (PMT).

The Hamamatsu R5783P-01 photosensor module, which is based on the R5600P-01 ''metal package'' photomultiplier, has been used for all reported time-resolved measurements. The photomultiplier is very fast, has a gain of up to 10^6, and is guaranteed to be linear within 1% for signals that are up to 10 times stronger than those measured in this investigation.

Time-integrated measurements are done by measuring the photomultiplier output using a LeCroy 612A charge integrator. Time-resolved measurements are done on a Hewlett Packard HP54111D digitizing oscilloscope that is connected to the PMT anode with a 50 Ω coaxial cable. The oscilloscope samples at 1 GHz and has a bandwidth of 500 MHz. Figure 2 shows the averaged single photon response of the photosensor module as measured with the oscilloscope. This data has been used to deconvolute the measured fluorescence decay data. The main peak has a full width at half maximum (FWHM) of about 1.5 ns, significantly shorter than the fluorescence decay time of 10 ns.

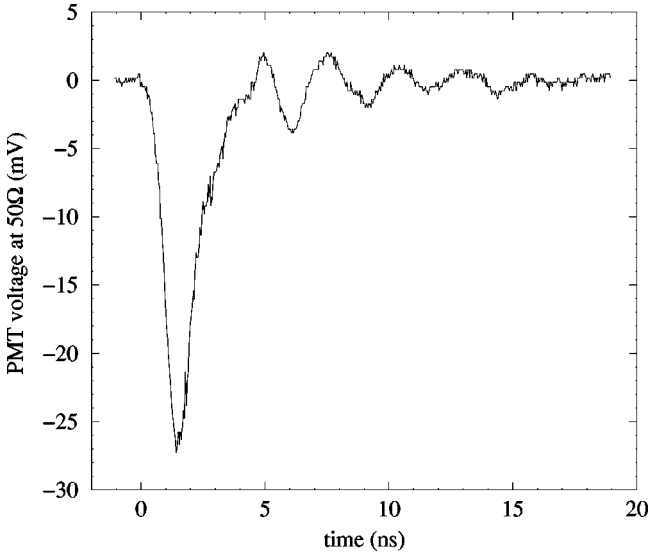

FIG. 2. Averaged single photon response of the R5783P-01 photosensor module.

III. EXPERIMENTAL RESULTS AND DISCUSSION

Even in the absence of quenching, it is not immediately obvious what the radiatively governed decay time of the H $p=3$ state should be. Due to two-photon selection rules the laser can only create excited $3s$ and $3d$ substates. The actual fluorescence decay time now depends on the channels for de-excitation that are available to those substates. There are two general scenarios: (i) the substates remain isolated, in which case the $3s$ and $3d$ populations will decay with a natural lifetime of 159 and 15.5 ns, respectively (see Table I for a list of radiative transition frequencies and decay times), and (ii) there is a coupling between the $3s$, $3p$, and $3d$ substates, so that these states will be mixed and populated according to their respective statistical weights, and the decay time will be the average radiative decay time of 10 ns. Note that in the calculation of the averaged decay time, it was assumed that the densities are sufficiently low to prevent

TABLE I. Radiative transition frequencies and lifetimes for the $p=3$ sublevels and average value of all sublevels [13].

Transition	A $(10^8$ $s^{-1})$	$\tau(10^{-9}$ s)
$3s\rightarrow 2p$	0.0631	158.5
$3p\rightarrow 2s$	0.2245	44.45
$3p\rightarrow 1s$	1.672	5.981
$3d\rightarrow 2p$	0.645	15.50
avg. $3\rightarrow 1,2$	0.998	10.02

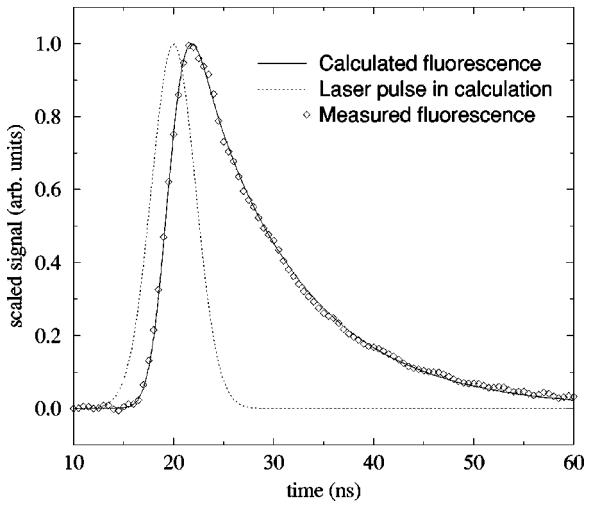

FIG. 3. Comparison of the modeled response (solid curve) with a deconvoluted measurement at $z=2$ cm distance from the arc nozzle (diamonds). The Gaussian function with a peak at 20 ns represents the modeled laser intensity (a.u.).

trapping of resonant Lyman radiation in the detection volume.

In Fig. 3 we present a typical deconvoluted observed H fluorescence signal. The measurement was done at 2 cm from the nozzle. After deconvolution, the decay time was obtained using an exponential fit resulting in a value of 10.3 ± 0.5 ns.

Figure 4 shows the result of a measurement of the fluorescence decay time at various positions along the expansion symmetry axis. The decay times were again obtained by computer fits to the deconvoluted time-resolved signals. The errors in the values are about 0.5 ns.

The fact that a decay time of 10 ns is found indicates that a fast mechanism exists that mixes the excited $3s$, $3p$, and $3d$ states so that all $p=3$ substates are populated according to statistical weights [scenario (ii)]. One might argue that the natural decay time is in reality 15.5 ns (from the $3d \rightarrow 2p$ transition) and that the observed fluorescence is quenched to 10 ns, but this can be discarded since the same decay time

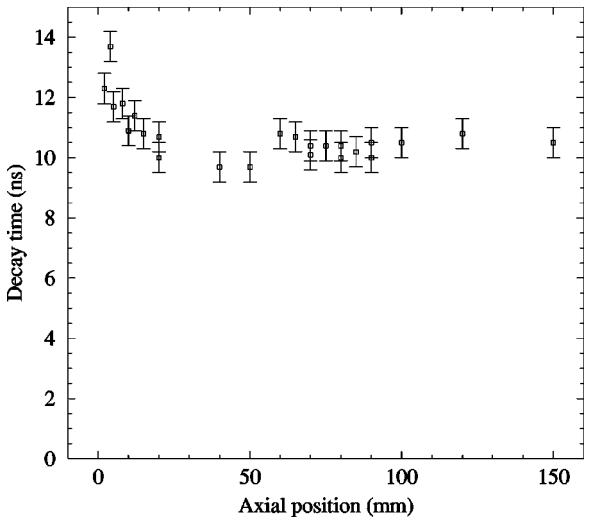

FIG. 4. Fitted decay times of the deconvoluted time-resolved fluorescence signals as a function of axial position.

has been found for a large range of ground state and electron densities. Close to the arc nozzle (positions 0–10 mm), the decay times seem to be slightly higher. This might be caused by resonant Lyman-β radiation trapping in the plasma region with relatively high H density ($\approx 10^{21}$ m^{-3}). Otherwise all decay times are near 10 ns, so the measurements show no signs of quenching.

In the work of Preppernau *et al.* [11], H $p=3$ lifetime measurements were performed, where hydrogen atoms were created by photodissociating C_2H_2. At low C_2H_2 pressures (≈ 10 mTorr) a lifetime of 15.7 ± 1.5 ns— corresponding to scenario (i) — was found using a computer fit, while at 150 mTorr the lifetime is close to 10 ns. The authors fit the experimental lifetime data with a model in which the collisional quenching effects are split up into a sublevel mixing rate and a rate for collisional deexcitation of all $p=3$ sublevels. In our case, the sublevel mixing could be caused by unscreened electric fields that do not extend outside the Debye sphere or by the laser beam electric field, both of which are not considered in the model described in Ref. [11].

IV. MODELING

A. Basic setup

As was discussed in Sec. II, it is expected that the cascaded arc plasma source dissociates a large part of the H_2 molecules. For the calculations we therefore assume that the influence of laser induced excitation of hydrogen atoms can be adequately described by modeling the hydrogen atomic system and ion ground state only. It has been experimentally verified that the laser causes no significant H_2 dissociation [6].

The basis of collisional radiative models is the particle balance equation for the density n_p of atoms in level p:

$$\frac{\partial n_p}{\partial t} + \nabla \cdot n_p \vec{w} = \sum_{q \neq p} (n_q F_{qp} - n_p F_{pq}), \tag{1}$$

where $\vec{w}$ is the flow velocity and F_{pq} the total frequency of transitions from p to q, with $p,q = 1,2,\ldots,m,+$ (ion). Equation (1) relates the temporal ($\partial/\partial t$) and spatial (∇) changes in state density to the net result of all elementary population (positive term in the summation) and depopulation (negative term) processes.

The frequency F_{pq} is generally given by

$$F_{pq} = n_e K_{pq} + \Lambda_{pq} A_{pq}, \tag{2}$$

with n_e the electron density, K_{pq} the coefficient for electron collision induced transitions (calculated following Vriens and Smeets [12]), Λ_{pq} the escape factor and A_{pq} ($p>q$) the Einstein coefficient for a radiative transition [13]. Resonant radiation trapping has not been included in the model, since at typical hydrogen densities ($<10^{21}$ m^{-3}) the photon mean free path is several orders of magnitude larger than a typical dimension of the detection volume, so all Λ_{pq}'s are set to unity.

A special case is K_{+q}, which consists of two and three particle recombination parts with coefficients $K_{+q}^{(2)}$ and $K_{+q}^{(3)}$, respectively,

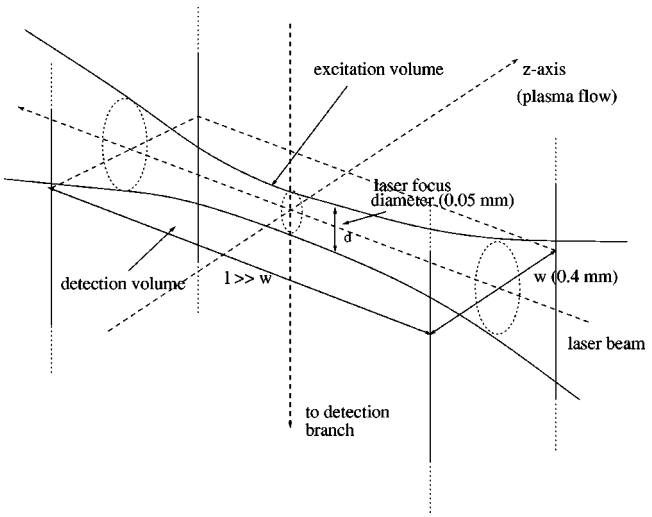

FIG. 5. Overview of the excitation and detection volumes. The plasma expands in the z direction. The relevant dimensions for the excitation and detection volumes are d ($\approx$0.05 mm) and w (0.4 mm), respectively.

$$n_e K_{+q} = n_e K_{+q}^{(2)} + n_e^2 K_{+q}^{(3)}. \tag{3}$$

The number of levels described by the model is limited using a cutoff procedure which is based on the analytically well-known step-wise ionization-recombination process [5]. The following subsection will discuss the implications of the spatial term in Eq. (1). After that, the description of the temporal laser interaction will be discussed.

B. Spatial effects

The main concern of this section has to do with the fact that only atoms in a very small part of the plasma (the excitation volume) are excited, and that only a limited ''slice'' of plasma is monitored for fluorescence (the detection volume). Figure 5 shows an overview of both the excitation and the detection volume. The smallest dimension in the detection volume is the detection slit width w (0.4 mm) and in the excitation volume it is the laser focus diameter d (about 50 μm). These dimensions are typically smaller by at least an order of magnitude than collisional free path lengths, so heavy particle collisions will play no role in the following discussion.

For the duration of the laser pulse ($\sim$5 ns), all excited H atoms are confined to the excitation volume, i.e., there is no significant out-flux of excited atoms and in-flux of ground state atoms, as can be seen from the following argument. Using a worst-case temperature of 3000 K, the thermal velocity is $\sqrt{kT/m_H} = 5 \times 10^3$ m/s. In 5 ns a distance of 25 μm is traveled, half the laser focus diameter. We therefore ignore the spatial term for at least the duration of the laser pulse.

After the laser pulse, the excited particles will continue to spread over an increasing volume due to the thermal motion. At thermal velocities, particles will start leaving the detection volume after about 40–80 ns.

It is important to realize at this point that the fluorescence signal is actually not proportional to the density n_3 of the exited state, but to the number of excited particles $N_3 = \int_{V_d} n_3 dV$ in our detection volume V_d. Integrating Eq. (1) over the detection volume gives

$$\frac{\partial N_p}{\partial t} = \sum_{q \neq p} (N_q F_{qp} - N_p F_{pq}), \tag{4}$$

where we used $\int_{V_d} \nabla \cdot n_p \vec{w} dV = 0$ as long as the excited particles are confined to the detection volume. Equation (4) has the same structure as Eq. (1) without the spatial term, which effectively describes an infinite cross-section laser beam and an infinite detection volume. A solution for this simplified system is therefore appropriate for the description of a LIF experiment. However, it is important to note that F_{pq} in Eq. (4) still depends on n_e, as can be seen from Eq. (2). In the remainder of this section we will consider how the electron and ion densities are affected.

As we shall see in Sec. V, the laser is capable of drastically increasing ion and electron densities, and it is important for the modeling of the fluorescence decay to correctly describe the relaxation of the increased densities. Moreover, since the photoionization from $p=2$ only requires 3.4 eV and the laser photons carry 6 eV, even the local electron temperature will be affected. Equation (5) gives an expression for a weighed time-dependent electron temperature:

$$T_e(t) = \frac{n_e(0) T_e(0) + [n_e(t) - n_e(0)] \times 3\text{eV}}{n_e(t)}, \tag{5}$$

with $n_e(0), T_e(0)$ the initial electron density and temperature and using an average electron energy after photoionization of 3 eV.

If the Debye length λ_D is much larger than a typical dimension of the detection volume ($w = 0.4$ mm), the electrons leave this volume with the thermal velocity $\sqrt{kT_e/m_e}$. In the current plasma, with $n_e < 10^{19}$ m^{-3}, the opposite is the case so even with $T_e \approx 3$ eV for the new electrons, λ_D is only several μm and thus smaller than a typical detection dimension. The electrons will thus disappear at ion acoustic velocity $\sqrt{kT_e/m_H}$, with a characteristic time of between 3 ns (high energy electrons at 3 eV) and 10 ns (slow electrons at 0.3 eV). In the calculations, an electron density decay time of 5 ns has been used.

C. Temporal effects

In the preceding section we have seen that we can ignore the spatial terms except for the electron and ion densities. The system of density equations (4) can then be written as a single matrix equation of the form

$$\frac{\partial}{\partial t} \vec{n} = M \cdot \vec{n}, \tag{6}$$

with $\vec{n}$ a vector of all densities $n_1 \cdots n_+$ and

$$M_{pq} = \begin{cases} F_{qp}, & p \neq q, \\ -\sum_{r \neq p} F_{pr}, & p = q. \end{cases} \tag{7}$$

In the steady state (SS) approximation, the densities n_1 and n_+ have an imposed value [this can be easily incorpo-

rated in Eq. (6)] and all time derivatives are set to zero. The SS density distribution is then calculated using a straightforward matrix inversion.

For a time-dependent calculation of the effects of a short disturbance of the system (as caused by a laser pulse) we first calculate the SS solution $n(t=0)$. This solution is then used as the initial condition for the differential equation $(\partial/\partial t)\vec{n}(t)=M(t)\cdot\vec{n}(t)$, which is solved using a fourth order Runge-Kutta method [14]. The time-dependence of matrix M is discussed below.

In describing two-photon laser-induced hydrogen excitation, we make no distinction between $1s\rightarrow 3s$ and $1s\rightarrow 3d$ transitions. As we have experimentally found, there is a fast coupling between the $3s$, $3p$, and $3d$ levels, so that always $\eta_{3s}=\eta_{3p}=\eta_{3d}$, where $\eta_x=n_x/g_x$.

Laser-induced excitation of ground state atoms to the $p=3$ level introduces an additional term in F_{13} and F_{31}. For a two-photon transition this contribution is given by [15,16]

$$\delta F_{13}=\frac{\zeta_{13}^{(2)}P_\nu}{h\nu}G\langle I(t)\rangle^2 \tag{8}$$

and $\delta F_{31}=(g_1/g_3)\delta F_{13}$, with $\zeta_{13}^{(2)}$ the two-photon excitation cross section divided by the spectral line-width function and the two-photon statistical factor $[\mathrm{m^4\,s^{-1}\,W^{-1}}]$, ν the laser frequency, G a statistical factor that is generally 2 for dye lasers [15], I the laser intensity $[\mathrm{W\,m^{-2}}]$ and P_ν the result of a convolution of laser and Doppler line profiles. The value for $\zeta_{13}^{(2)}$ is the weighted average of $\zeta_{1s\rightarrow 3s}^{(2)}$ $(2.42\times 10^{-18}\ \mathrm{cm^4\,s^{-1}\,W^{-1}})$ and $\zeta_{1s\rightarrow 3d}^{(2)}$ $(18.3\times 10^{-18}\ \mathrm{cm^4\,s^{-1}\,W^{-1}})$ [15,17].

We also have to take laser induced ionization into account as a depopulation mechanism of the excited levels. The cross section for ionization σ_{p+} of level p for hydrogen atoms is given as a function of the laser frequency ν by [18]

$$\sigma_{p+}(\nu)=2.815\times 10^{29}\ \mathrm{cm^2\,s^{-3}}\frac{1}{\nu^3 p^5}, \tag{9}$$

with contributions to the frequency matrix

$$\delta F_{p+}=\frac{\sigma_{p+}\langle I(t)\rangle}{h\nu}. \tag{10}$$

This laser induced ionization needs to be included when $\delta F_{p+}>\Sigma A_{pq}$, and because of the p^{-5} dependency, this only holds for the $p=2,3$ states, using $I_{\max}\approx 10^9\ \mathrm{W\,cm^{-2}}$.

To describe the changes in electron and ion densities, caused by effects discussed in the previous section, we add an extra term to the equation for the ion density

$$\frac{\partial n_+}{\partial t}=(M\cdot\vec{n})_+-\frac{[n_+-n_+(0)]}{\tau}, \tag{11}$$

with $n_+(0)$ the steady state ion density and $\tau=5$ ns the relaxation time. Finally, we can choose to keep the electron density and ion density equal, $n_e(t)=n_+(t)$, or allow the electrons to escape instantaneously, $n_e(t)=n_e(0)$, corresponding to the cases of $\lambda_D \ll w$ and $\lambda_D \gg w$, respectively.

D. Calculated values

The model described above allows us to plot the state densities as a function of time. To be able to use the model to predict the outcome of a typical two-photon LIF experiment where time-integrated LIF signals are recorded it is necessary to calculate a number that represents total integrated fluorescence yield.

The average number of fluorescence photons emitted per atom after laser excitation N_γ is given by [15]

$$N_\gamma=\frac{A_{32}}{n_1(0)}\int_0^\infty [n_3(t)-n_3(0)]dt, \tag{12}$$

with A_{32} the fluorescence transition probability. In an ideal LIF experiment, the amount of detected fluorescence will be proportional to n_1. One of the aims of the model is to calculate under which plasma parameters this holds. The average number of photons per atom (N_γ) is an important parameter if we want to measure (relative) atomic densities in different parts of the plasma. The implication to the applicability of LIF is that the ratio of two independently obtained LIF signals is not necessarily equal to the ratio of the respective H ground state densities if the relevant N_γ values are not known to be equal. Moreover, since the fluorescence usually is calibrated to the ground state density using another plasma [6], it is very important to know the behavior of N_γ.

V. RESULTS AND DISCUSSION

A. Calibration of the model laser intensity

This section describes a few measurements that were done to gain more knowledge about the laser pulse time profile and peak intensity. The results of a measurement and a calculation of the hydrogen fluorescence yield as a function of the laser intensity will be compared to determine the actual average laser pulse intensity.

In order to experimentally obtain the average laser intensity as a function of time $I(t)$, the temporal shape of the profile was measured using a fast SiC photodiode. A slightly asymmetrical Gaussian profile with a FWHM value of 5.2 ± 0.3 ns was observed.

A frequency-tripled Nd:YAG pumped dye laser has a considerable spread in pulse energies, due to pulse to pulse fluctuations. By measuring the pulse energy and the time-integrated fluorescence signal pulse by pulse, it is possible to use this spread to plot fluorescence signal as a function of laser energy without actively adjusting the laser power. Figure 6 shows the result from such a measurement with an average laser pulse energy of 0.5 mJ. The vertical distances between the horizontal ticks give the standard deviation of the fluorescence signal, while the error bars signify the standard deviation in the mean of the fluorescence signal. The average laser pulse energy and its standard deviation are given by the vertical lines. Figure 6 indicates that we are operating not far from saturation.

A model calculation is used to find out what the corresponding laser intensity is. The calculations are made with typical expansion plasma parameters $n_1=10^{20}\ \mathrm{m^{-3}}$, $n_+=n_e=2\times 10^{18}\ \mathrm{m^{-3}}$, and $T_e=0.3$ eV. Figure 7 shows the calculated N_γ values as a function of laser intensity I for the

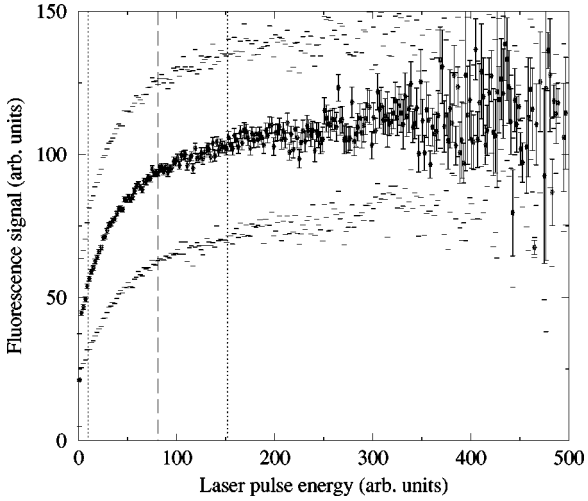

FIG. 6. Measured time-integrated fluorescence signal as a function of laser pulse energy measured by a SiC diode. The ticks and error bars represent standard deviations in signal and mean signal, respectively. The average laser pulse energy and its standard deviation are given by the vertical lines.

cases of disappearing laser generated electrons (solid curve) and remaining electrons (dotted curve). In the latter case, the maximum N_γ value is significantly lower, because with sufficiently high intensity the laser beam creates enough electrons, through ionization of excited H atoms, to quench the excited $p=3$ density.

Up to $I=10^8$ W cm^{-2}, N_γ is proportional to I^2, for higher laser intensities N_γ reaches a saturation value. The decrease at still higher intensities is caused by increased competition of laser induced ionization of the excited $p=3$ states, thereby reducing the fluorescence quantum yield. Comparing Fig. 6 to Fig. 7 we estimate that the effective laser intensity under experimental conditions is about 4×10^8 W cm^{-2}.

B. Calculations

In Fig. 3 a comparison is shown between a modeled time profile and an experimentally observed one. The modeled

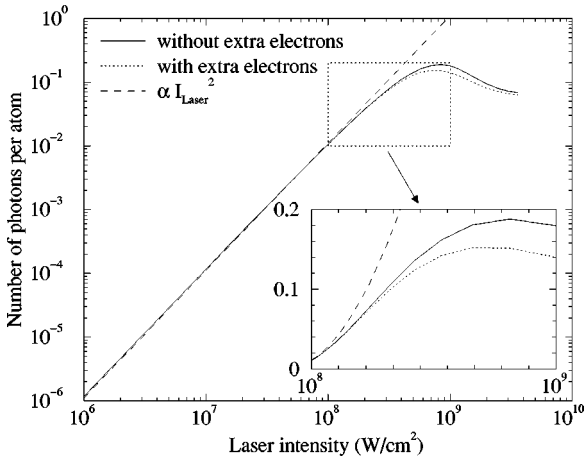

FIG. 7. N_γ as a function of laser intensity (log-log scale) for the cases of disappearing laser generated electrons (solid curve) and remaining electrons (dotted curve). In the latter case, the maximum N_γ value is significantly lower. The inset shows the saturation region on a linear-linear scale.

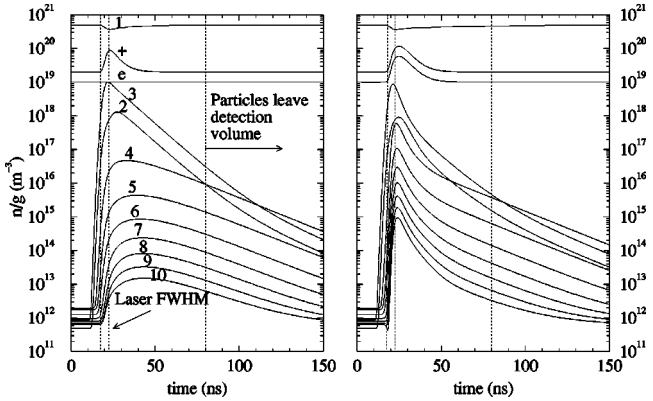

FIG. 8. Relative populations (n_p/g_p) of the first 10 hydrogen levels and the ion state $(+)$ as a function of time during and after pulsed laser excitation of the $p=3$ level. In the graph on the left, the laser produced electrons disappear instantly while in the right graph the electrons flow away with an imposed relaxation time of 5 ns. These electrons cause a notable quenching of the laser enhanced $p=3$ density.

response was calculated using parameters $n_1=10^{20}$ m^{-3}, $n_+=n_e=2\times10^{18}$ m^{-3}, and $T_e=0.3$ eV. The measurement was done at 2 cm from the nozzle. The modeled and measured temporal fluorescence shapes are in good agreement.

Figure 8 shows the calculated relative populations (n_p/g_p) of the first ten atomic H levels and the ion level as a function of time during and after pulsed laser excitation of the $p=3$ level, for an initial ground-state density $n_1=5\times10^{19}$ m^{-3} and electron density $n_e=n_+=2\times10^{18}$ m^{-3}. The electron temperature is taken to be 0.3 eV and the laser pulse has a maximum at the chosen time $t=20$ ns. The left and right graphs correspond to calculations with instantly disappearing electrons and remaining energetic electrons, respectively. In the latter case, the surplus electrons flow away with a characteristic time of 5 ns and T_e is given by Eq. (5).

The laser interaction causes a radical change in densities through the entire atomic system, since a substantial part of the ground state population is pumped to level $p=3$, and via this level to other regions of the excitation space. One benefit of this effect is that the results of the calculation will not be influenced strongly by an error in the steady state density distribution at the start.

Note the significant increase in the ion density (a factor of 5). The laser has therefore a profound, albeit temporary, influence on the local electron density. The calculation without laser generated electrons shows similar time profiles for the ground state, the ion state, and the first two excited levels, and significantly lower (by at least an order of magnitude) populations of the other excited levels. In the right graph, the temporarily increased electron density and temperature raises the process of collisional excitation from the $p\leqslant3$ to the $p>3$ levels.

Also note the difference in the $p=3$ decay time for the two situations. In the left graph the decay time is 10 ns, purely governed by radiative processes, while in the right graph the decay is clearly much faster, resulting in a quenching of the fluorescence. As was explained in Sec. IV D, it is useful to use the model to calculate how the value of N_γ depends on the plasma parameters, so that we may determine

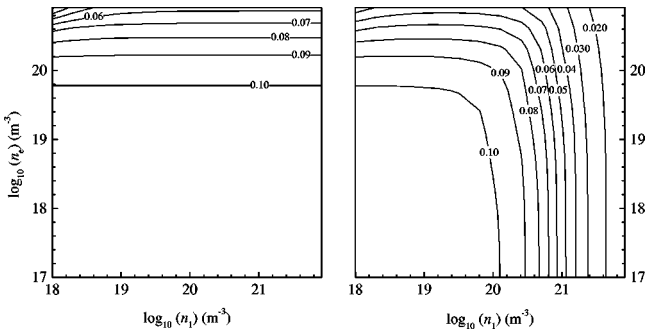

FIG. 9. Contour plots of the calculated N_γ as function of $n_+ = n_e$ and n_1, for $T_e = 0.3$ eV with instantly disappearing laser generated electrons (left) and slowly flowing electrons, with characteristic decay time 5 ns, (right). If n_1 is higher than 10^{20} m^{-3} the laser produces enough electrons to quench the laser enhanced $p=3$ density, thereby reducing the N_γ value.

how well measurements in different parts of the plasma can be compared.

Assuming $n_+ = n_e$, we have three variables n_e, n_1, and T_e. The electron density was varied between 10^{17} and 10^{21} m^{-3}, the atom density between 10^{18} and 10^{22} m^{-3} and the electron temperature was 0.3 eV. Figure 9 shows the results of the calculations in the form of a contour plot for again the case of disappearing (left) and remaining laser generated electrons (right).

Without laser generated electrons, N_γ is constant for all values of n_1 with $n_e < 10^{20}$ m^{-3}. The decrease in N_γ for $n_1 > 10^{20}$ m^{-3} in the right graph is caused by a ''self-quenching'' effect; the ion production becomes so large, through photoionization, that the electron density increases enough for electron collisions to become a major factor in the depopulation, even though the surplus electrons flow away with a relaxation time of 5 ns.

VI. CONCLUSIONS

In this article we presented an experimental as well as a computational study on the effect of pulsed laser excitation on a hydrogen plasma as is, e.g., the case in two-photon LIF experiments for the measurement of ground state H densities. We found no quenching of the H $p=3$ state in the time-resolved fluorescence measurements in the expanding cascaded arc plasma. The fact that we found a constant decay time of 10 ns, indicates the existence of an *l*-mixing mechanism in the expanding plasma. There is good agreement between the shapes of the measured and calculated time-resolved fluorescence of the $p=3$ level, which indicates that (1) the laser intensity time-profile was modeled accurately enough, (2) the deconvolution procedure works adequately as well, and (3) the fluorescence signal shape is not very dependent on the exact initial $p=3$ population.

Model calculations indicate that a potential problem for the diagnostic application of two-photon LIF for the measurement of atomic H densities is self-quenching, i.e., quenching of the laser excited states by electrons that were created through laser induced ionization. It is especially important to consider this effect since two-photon LIF is usually thought of as a nonintrusive technique.

As was mentioned before, an important parameter is the ratio between the plasma Debye length and a characteristic length of the detection volume. If this ratio is much larger than one, the created energetic electrons can quickly spread from the excitation volume over the entire Debye sphere, so that the additional density in the detection volume is reduced. The ions will not spread so quickly, but since recombination is a relatively slow process, an increased ion density does not affect the excitation kinetics much.

If the Debye length is much smaller than the smallest dimension of the detection volume, the laser-freed electrons will stay around the excited atoms in the excitation volume, and might seriously interfere with the fluorescence signal by causing extra collisional depopulation. Our calculations show that, with a laser intensity of 4×10^8 $W\,cm^{-2}$, this happens at $n_1 > 10^{20}$ m^{-3}. Since this value for the laser intensity is a realistic one in the case of nonattenuated focussed laser beams, it is strongly recommended to work with moderate laser intensities. In the case of two-photon LIF measurements in H this should certainly be feasible considering the relatively strong two-photon cross sections. Moreover, the occurrence of (self-) quenching can be readily checked in a time-resolved LIF experiment since the fluorescence quantum yield is directly proportional to the life time of the excited state.

ACKNOWLEDGMENTS

The authors gratefully acknowledge Professor Dr. H. F. Döbele (Institute for Laser- and Plasma Physics, Essen University, Germany) for his vital contribution in the initial phase of the two-photon LIF experiments in Eindhoven. We also thank H. M. M. de Jong, M. J. F. van de Sande, and A. B. M. Hüsken for their skillful technical assistance. A. Hartgers wrote the collisional radiative model that was used as a basis for the model in the present work. This work is part of the research program of the ''Stichting voor Fundamenteel Onderzoek der Materie (FOM),'' which is financially supported by the Nederlandse Organisatie voor Wetenschappelijk Onderzoek (NWO), and is also financially supported by the Dutch Technology Foundation STW.

[1] J. Bokor, R. Freeman, J. White, and R. Storz, Phys. Rev. A **24**, 612 (1981).
[2] W. Bischel, B. Perry, and D. Crosley, Chem. Phys. Lett. **82**, 85 (1981).
[3] M. Heaven *et al.*, Chem. Phys. Lett. **86**, 458 (1982).
[4] S. Hansen, G. Luckman, G. Nieman, and S. Colson, Appl. Phys. Lett. **51**, 898 (1987).
[5] J. van der Mullen, Phys. Rep. **191**, 109 (1990).
[6] M. Boogaarts *et al.* (unpublished).
[7] M. van de Sanden *et al.*, Rev. Sci. Instrum. **63**, 3369 (1992).

[8] M. van de Sanden *et al.*, Surf. Coat. Technol. **74-75**, 1 (1995).
[9] M. van de Sanden *et al.*, Plasma Sources Sci. Technol. **5**, 268 (1996).
[10] S. Mazouffre, M. Boogaarts, J. van der Mullen, and D. Schram, Phys. Rev. Lett. (to be published).
[11] B. Preppernau *et al.*, Chem. Phys. **196**, 371 (1995).
[12] L. Vriens and A. Smeets, Phys. Rev. A **22**, 940 (1980).
[13] W. Wiese, M. Smith, and B. Miles, *Atomic Transition Probabilities* (National Bureau Standards, Washington, D.C., 1969).
[14] *Numerical Recipes in C — The Art of Scientific Computing*, edited by W. Press (Cambridge University Press, Cambridge, 1992).
[15] U. Czarnetzki *et al.*, J. Opt. Soc. Am. B **11**, 2155 (1994).
[16] J. Amorim, G. Baravian, M. Touzeau, and J. Jolly, J. Appl. Phys. **76**, 1487 (1994).
[17] J. Tung, A. Tang, G. Salamo, and F. Chan, J. Opt. Soc. Am. **3**, 846 (1986).
[18] *Plasma Diagnostics*, edited by Lochte-Holtgreven (Elsevier North-Holland, Amsterdam, 1968).